An automated processing chain for the retrieval of georeferenced reflectance data from hyperspectral EO-1 HYPERION acquisitions

Christian Rogass[1], Luis Guanter[1], Christian Mielke[1], Daniel Scheffler[1], Nina K. Boesche[1],

Christin Lubitz[1], Maximilian Brell[1], Daniel Spengler[1] and Karl Segl[1]

1. Helmholtz Centre Potsdam GFZ German Research Centre for Geosciences, Section Remote Sensing, Potsdam, Germany; emails: christian.rogass,luis.guanter,christian.mielke,daniel.scheffler,nina.boesche,christin.lubitz, maximilian.brell,Daniel.spengler, karl.segl (@gfz-potsdam.de)

ABSTRACT

Spaceborne hyperspectral imaging becomes more and more important for remote sensing applications. Data acquisitions from current sensors having VNIR and SWIR detectors, like Hyperion on the EO-1 platform, and future sensors, such as EnMAP, MSMI, HISUI, Prisma or HyspIRI, require precise data pre-processing to enable the variety of applications they are designed for. Most applications require continuous spectra over the VNIR and SWIR wavelength range (e.g. geological applications) and georeferenced reflectance as data process level to be independent of illumination and sensor geometry, to reduce the influence of the atmosphere during the acquisition and to enable the integration of application related outputs information into spatially larger georeferenced information systems.

In this work, an automated pre-processing chain for EO-1 Hyperion data acquisitions is presented that aims on providing georeferenced reflectance data. As input serves only L1 radiance data, L1T radiance terrain corrected data, a DEM and some metadata which are freely distributed through the USGS Earth Explorer web portal. Data processing comprises rescaling of the data, removal of the spectral overlap, bad band detection, reductions for dead pixel and erroneous detector columns, intra-band spatial shifts, keystone, erroneous co-registration, radiometric miscalibration as well as the radiative transfer modelling assisted atmospheric correction that also accounts for spectral smile. Georeferencing is performed after reflectance retrieval to exclude resampling effects from the atmospheric correction. First results are presented that demonstrate the potential of the new pre-processing chain. The achieved high data quality and new data products will promote a higher interest and broader usage of the freely distributed EO-1 Hyperion data takes.

INTRODUCTION

Remote sensing and especially its performing branch – the imaging spectroscopy – enable a broad variety of geospatial applications that mostly integrate environmental, economic and social aspects. The future German hyperspectral mission - Environmental Mapping And Analysis Program (EnMAP; [1,2]) – whose launch is planned for late 2017 will play a key role due to its capacity to acquire hyperspectral images of high spatial, radiometric and spectral quality (about 150’000 km² per day). Currently, algorithm development for data pre-processing and scientific exploitation is ongoing. In this context, data recorded by EnMAP analogous operating hyperspectral spaceborne sensors like NASA’s EO-1 Hyperion [3] are in particular important for this purpose. Therefore, the product quality of EO-1 Hyperion data is crucial for any succeeding algorithm development requiring an optimized pre-processing of georeferenced at-ground reflectance. Because current atmospheric and geometric correction approaches do not integrate a reduction of remaining keystone as proposed in [4], it was necessary to develop and to propose a

 ISBN 978-83-63245-65-8, DOI: 10.12760/03-2014-06, Zagajewski B., Kycko M., Reuter R. (eds.)

new processing chain for EO-1 Hyperion that is described in the following. It has been fully automatized using the inputs that are provided by the data supplier (USGS).

THE PROCESSING CHAIN

For the development of the Hyperion processing chain hundreds of Hyperion scenes have been utilized. In this work, the chain is exemplarily described using only one Hyperion scene. The scene was acquired at 17:53 o'clock on the 23th of February 2003 over the city of Phoenix, Arizona, USA (Scene-ID EO1H0370372003054110PW) incorporating a sun azimuth of about 144° and a sun elevation of about 40°. The location of the flight strip is shown in figure 1.

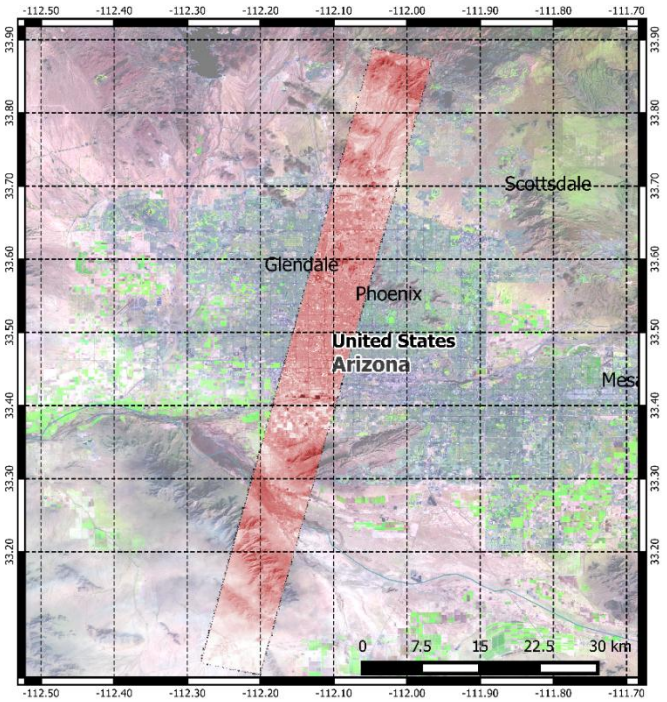

Figure 1: Location of the exemplary EO-1 Hyperion scene as reddish transparent overlay of a Landsat-7 scene (Scene-ID LE70370372003054EDC00) and related geographic information layer

Two processing levels of EO-1 Hyperion have been utilized – L1R and L1T. L1R is level 1 radiance and radiometrically corrected and not georeferenced. L1T is like L1R but additionally orthorectified and geocoded (UTM projection). The data set was complemented with an MTL file that contains necessary meta data information like acquisition date, time, angles, bounding box etc. In addition to the Hyperion data set a DEM (Digital Elevation Model) is necessary to reduce uncertainties in the process of geometric correction that can be induced by the impact of rough terrain on the perspective scan line acquisition. In this work a UTM re-projected ASTER DEM has been utilized. All used data sets have been obtained beforehand through the USGS Earth Explorer web portal (http://earthexplorer.usgs.gov/; accessed on 13.06.2014). The processing chain consists of six modules that are named and shown in figure 2. In the first module – input – all information is collected and prepared for processing in succeeding modules.

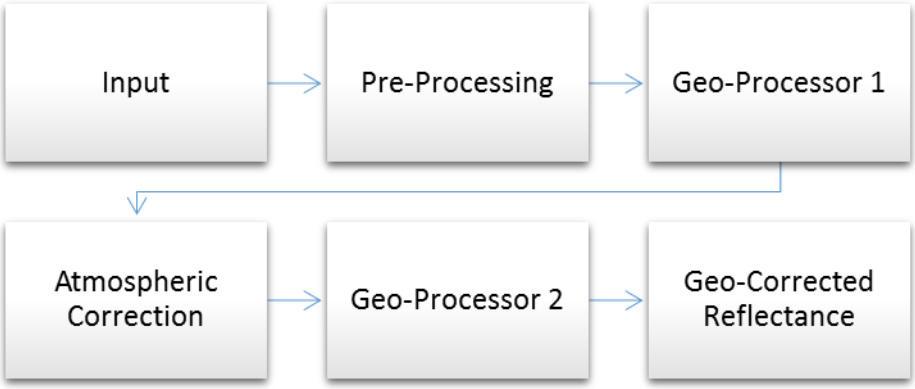

Figure 2: Hyperion processing chain

In the second module – pre-processing – a set of reduction and correction algorithms are applied. This comprises:

- Rescaling to radiance, Half SWIR shifting and Erroneous pixel and column reduction
- Reduction of radiometric miscalibration
- Keystone reduction
- Cloud masking

The rescaling to radiance is used to retrieve physical units – radiance. This is performed by a division of all VNIR bands (1 – 70) with 40 and all SWIR bands (71-242) with 80 as suggested in [5]. Then, the SWIR is half backward shifted by one pixel as suggested by [6]. In a next step erroneous pixel are reduced applying a new developed and fast approach. For this, the bad pixel mask that is part of the data set is utilized. First, a broad boxcar of 9x9 elements is applied to retrieve a spatially smoothed representation of the original image cube whereas erroneous pixel are excluded from the computation. Then, all erroneous pixel values are substituted by the pixel values from the smoothed representation. Other, approaches such as diffusion approaches [7] may work as well. After this erroneous columns are corrected using the approach of [8]. Next, the reduction of radiometric miscalibration is applied that is similar to those proposed in [9,10] but additionally minimizes across track gradients. The keystone reduction is similar to the approach proposed in [4]. Stationary deviations of the line-of-sight between adjacent spectral bands are assumed as local gradient deviations between adjacent bands and are least squares modelled on locally estimated distortions within small arbitrary windows. Those windows are centered around automatically detected tie points derived using the approach of [11]. Contemporarily, a global distortion minimization as proposed in [12] is applied as intrinsic validation to iteratively improve foregoing least squares distortion models. The final distortion model is then inverted and applied on the original L1R data using bicubic interpolation, whereas the polynomial modelling has still potential for improvements as exemplarily shown in figure 3.

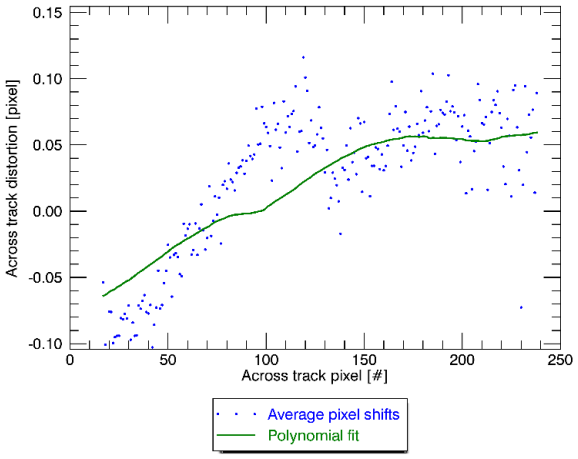

© EARSeL and University of Warsaw, 2014, ISBN 978-83-63245-65-8, DOI: 10.12760/03-2014-06, Zagajewski B., Kycko M., Reuter R. (eds.)

Figure 3: Relative across-track distortion between VNIR and SWIR (blue) and its polynomial model (green) of low degree

In the last step of the pre-processing a cloud mask is generated based on the L1R data. The cloud mask is retrieved as product of a hysteresis thresholded relative atmospheric oxygen absorption and a binary high albedo map as given in the following equation:

$$mask_{cloud} = \begin{cases} 1, m_2 \circ m_3 > 0 \\ 0, m_2 \circ m_3 = 0 \end{cases}$$

$$m_1 = \frac{L1R_{752.43\,nm} - L1R_{762.6\,nm}}{L1R_{752.43\,nm}}$$

$$m_2 = \begin{cases} 1, & L1R_{548.92\,nm} > L1R_{426.82\,nm} \\ 0, & L1R_{548.92\,nm} \leq L1R_{426.82\,nm} \end{cases}$$

$$m_3 = \begin{cases} 1, & m_1 \geq 0.7 * \max(m_1) \\ 0, & m_1 < 0.7 * \max(m_1) \end{cases}$$

where $\circ$ is the Hadamard product, m_1 the relative oxygen absorption due to increased scattering in the clouds, m_2 the binary albedo map due to reduced scattering induced reflection in the blue and m_3 the binary hysteresis of m_1 incorporating an arbitrary threshold. An exemplary result is shown in figure 4.

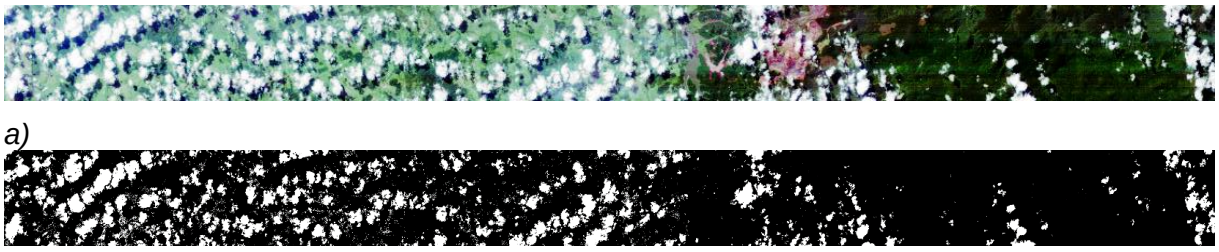

a)

b)

Figure 4: Color infrared composite of a cloudy Hyperion scene (a) and related result of proposed cloud masking approach as binary map

In the third module – Geo-Processor 1 – the geometric models for georeferencing and for co-registration are estimated using again the automatic tie point detection approach of [11]. In the first step, a DEM is extracted as subset of a larger DEM mosaic to serve as input for succeeding atmospheric correction. This is performed by projecting the L1T data set on the DEM mosaic. In the future complex ray tracing will be integrated to achieve higher accuracy for preceding corrections. In the second step, a coarse georeferencing is performed using the meta information like heading, altitude, earth rotation and average swath width that basically leads to scan line shifting and a rotation of the yaw axis. This coarse georeferenced L1R is then used as input for the SIFT tie point detection as proposed in [11]. This is also performed with the L1T data set that has been already georeferenced. Then, a locally window based Fourier-Mellin Transformation is conducted as proposed in [13] to determine local warping models comprising parameters for yaw rotation, scale and across- and along-track shifts. All those parameters are then used to determine a global polynomial model. This global polynomial model is then applied on the DEM subset. Hence, only the DEM is warped before atmospheric correction to enable reductions of sensor distortions like smile/frown during the atmospheric correction. In a last step, the co-registration is performed as proposed in [14] as EnMAP Co-Registration validation tool. For this purpose, a

polynomial model between spectrally adjacent bands of VNIR and SWIR is estimated using the tie points that have been previously determined during the keystone reduction.

After co-registration the L1R data is corrected for atmospheric influences as proposed in [15,16]. As input serves the L1R data set, the cloud mask, the projected DEM and some meta information on acquisition parameters. The atmospheric correction that has been utilized for Hyperion was originally designed for the EnMAP Box – the freely available software platform for the upcoming EnMAP mission as proposed in [17]. It includes a complex Radiative Transfer Modelling (RTM), Aerosol Optical Thickness (AOT) retrieval via the Dense Dark Vegetation Method (DDV), Columnar Water Vapour retrieval (CWV) similar to the Atmospheric Pre-Corrected Differential Absorption (APDA) algorithm of [18], Smile/Frown correction using atmospheric absorptions as in [16] and adjacency correction.

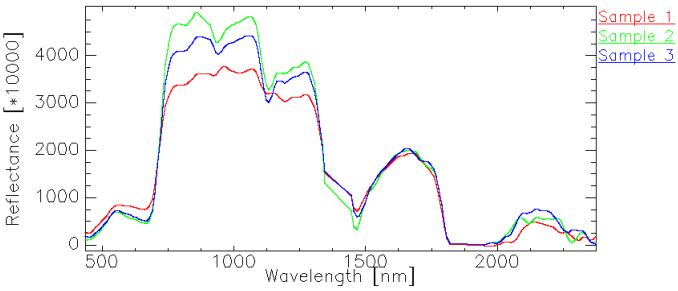

a) *b)*

Figure 5: Exemplary at-ground reflectance spectra of different vegetation species (a) and geocorrected at-ground reflectance spectra as false color composite overlay (CIR) on warped DEM of the central region of Phoenix, Arizona, U.S.

After atmospheric correction that transforms top-of-atmosphere radiance to at-surface reflectance data the Geo-Processor 2 starts. In this processor all geometric models of Geo-Processor 1 for coarse and fine georeferencing, relative keystone and co-registration are inverted and applied. Hence, geocorrected at-surface reflectance has been retrieved that builds the base for a variety of remote sensing applications as shown in figure 5.

CONCLUSION

In this work a new approach for the retrieval of at-surface reflectance from spaceborne hyperspectral EO-1 Hyperion acquisition is presented. It is fully automatized and has proven its performance in numerous application scenarios. Nevertheless, it is an ongoing development and there is still place for improvements. Those are e.g. the integration of ray tracing and sensor PSF projection for an improved re-sensing of the DEM and the L1R as in the EnMAP Simulator EETES of [19], a necessary spike polishing as in [20], runtime optimization and the validation of all modules.

ACKNOWLEDGEMENTS

This work was funded by the German Federal Ministry of Economics and Technology (BMWI 506 50EE1012/EnMAP) within the framework of EnMAP (Environmental Mapping and Analysis Program). We thank the U.S. Geological Survey's Earth Resources Observation and Science (EROS) Center for providing image samples.

REFERENCES

1. Sang, B.; Schubert, J.; Kaiser, S.; Mogulsky, V.; Neumann, C.; Forster, K.; Hofer, S.; Stuffler, T.; Kaufmann, H.; Muller, A. The EnMAP hyperspectral imaging spectrometer: instrument concept, calibration, and technologies. Imaging Spectrom. 2008, 13, 708605–708615.

2. Stuffler, T.; Förster, K.; Hofer, S.; Leipold, M.; Sang, B.; Kaufmann, H.; Penné, B.; Mueller, A.; Chlebek, C. Hyperspectral imagingâ€"An advanced instrument concept for the EnMAP mission (Environmental Mapping and Analysis Programme). Acta Astronaut. 2009, 65, 1107–1112.

3. Pearlman, J. S.; Barry, P. S.; Segal, C. C.; Shepanski, J.; Beiso, D.; Carman, S. L. Hyperion, a space-based imaging spectrometer. IEEE Trans. Geosci. Remote Sens. 2003, 41, 1160–1173.

4. Rogass, C.; Brell, M.; Segl, K.; Kuester, T.; Kaufmann, H. Automatic reduction of keystone - applications to EnMAP. In Proceedings of the 8th EARSeL SIG imaging spectroscopy workshop; EARSeL, 2013.

5. Beck, R. EO-1 User Guide v. 2.3; University of Cincinnati: Cincinnati, Ohio, U.S., 2003; p. 74.

6. Staenz, K.; Neville, R. A.; Clavette, S.; Landry, R.; White, H. P.; Hitchcock, R. Retrieval of surface reflectance from Hyperion radiance data. In Geoscience and Remote Sensing Symposium, 2002. IGARSS '02. 2002 IEEE International; 2002; Vol. 3, pp. 1419–1421 vol.3.

7. Perona, P.; Malik, J. Scale-Space and Edge Detection Using Anisotropic Diffusion. IEEE Trans Pattern Anal Mach Intell 1990, 12, 629–639.

8. Goodenough, D. G.; Dyk, A.; Niemann, K. O.; Pearlman, J. S.; Chen, H.; Han, T.; Murdoch, M.; West, C. Processing Hyperion and ALI for forest classification. IEEE Trans. Geosci. Remote Sens. 2003, 41, 1321–1331.

9. Rogass, C.; Spengler, D.; Bochow, M.; Segl, K.; Lausch, A.; Doktor, D.; Roessner, S.; Behling, R.; Wetzel, H. U.; Kaufmann, H. Reduction of radiometric miscalibration - applications to pushbroom sensors. Sensors 2011, 11, 6370–6395.

10. Rogass, C.; Spengler, D.; Bochow, M.; Segl, K.; Lausch, A.; Doktor, D.; Roessner, S.; Behling, R.; Wetzel, H. U.; Urata, K.; Hueni, A.; Kaufmann, H. A Contribution to the Reduction of Radiometric Miscalibration of Pushbroom Sensors. In Remote Sensing - Advanced Techniques and Platforms; Escalante-Ramirez, B., Ed.; InTech, 2012; pp. 151–170.

11. Lowe, D. G. Distinctive image features from scale-invariant keypoints. Int. J. Comput. Vis. 2004, 60, 91–110.

12. Rogass, C.; Segl, K.; Kuester, T.; Kaufmann, H. Performance of correlation approaches for the evaluation of spatial distortion reductions. Remote Sens. Lett. 2013, 4, 1214–1223.

13. Xie, H.; Hicks, N.; Keller, G. R.; Huang, H.; Kreinovich, V. An IDL/ENVI implementation of the FFT-based algorithm for automatic image registration. Comput. Geosci. 2003, 29, 1045 – 1055.

14. Rogass, C.; Brell, M.; Segl, K.; Kuester, T.; Kaufmann, H. AUTOMATED DETECTION OF SPATIAL DISTORTIONS OF HYPERSPECTRAL PUSH-BROOM SENSORS - APPLICATION TO THE ENMAP MISSION. In Proc. "ESA Living Planet Symposium 2013"; Edinburgh, UK, 2013; Vol. ESA SP-722, p. 6.

15. Guanter, L.; Richter, R.; Kaufmann, H. On the application of the MODTRAN4 atmospheric radiative transfer code to optical remote sensing. Int. J. Remote Sens. 2009, 30, 1407–1424.

16. Guanter, L.; Segl, K.; Sang, B.; Alonso, L.; Kaufmann, H.; Moreno, J. Scene-based spectral calibration assessment of high spectral resolution imaging spectrometers. Opt Express 2009, 17, 11594–11606.

17. Van der Linden, S.; Rabe, A.; Jakimow, B.; Held, M.; Leitao, P.; Hostert, P. The EnMAP-Box - a Toolbox for Imaging Spectroscopy Data Analysis and a Programming Interface for Application

Development. In Proc. “ESA Living Planet Symposium 2013”; Edinburgh, UK, 2013; Vol. ESA SP-722, p. 6.

18. Schläpfer, D.; Borel, C. C.; Keller, J.; Itten, K. I. Atmospheric Precorrected Differential Absorption Technique to Retrieve Columnar Water Vapor. Remote Sens. Environ. 1998, 65, 353–366.

19. Segl, K.; Guanter, L.; Rogass, C.; Kuester, T.; Roessner, S.; Kaufmann, H.; Sang, B.; Mogulsky, V.; Hofer, S. EeteS - The EnMAP End-to-End Simulation Tool. IEEE J. Sel. Top. Appl. Earth Obs. Remote Sens. 2012, 5, 522–530.

20. Gao, B.-C.; Liu, M. A Fast Smoothing Algorithm for Post-Processing of Surface Reflectance Spectra Retrieved from Airborne Imaging Spectrometer Data. Sensors 2013, 13, 13879–13891.